

Synchrotron Blob Model of Infrared and X-ray Flares from Sagittarius A*

Masaaki Kusunose

*Department of Physics, School of Science and Technology, Kwansai Gakuin University,
Sanda 669-1337, Japan*

kusunose@kwansai.ac.jp

and

Fumio Takahara

*Department of Earth and Space Science, Graduate School of Science, Osaka University,
Toyonaka 560-0043, Japan*

takahara@vega.ess.sci.osaka-u.ac.jp

ABSTRACT

Sagittarius A* in the Galactic center harbors a supermassive black hole and exhibits various active phenomena. Besides quiescent emission in radio and sub-millimeter radiation, flares in the near infrared (NIR) and X-ray bands are observed to occur frequently. We study a time-dependent model of the flares, assuming that the emission is from a blob ejected from the central object. Electrons obeying a power law with the exponential cutoff are assumed to be injected in the blob for a limited time interval. The flare data of 2007 April 4 were used to determine the values of model parameters. The spectral energy distribution of flare emission is explained by nonthermal synchrotron radiation in the NIR and X-ray bands. The model light curves suggest that electron acceleration is still underway during the rising phase of the flares. GeV γ -rays are also emitted by synchrotron self-Compton scattering, although its luminosity is not strictly constrained by the current model. If the GeV emission is faint, the plasma blob is dominated by the magnetic energy density over the electron kinetic energy density. Observations in the GeV band will clarify the origin of the blob.

Subject headings: acceleration of particles — black hole physics — Galaxy: center — radiation mechanisms: nonthermal

1. Introduction

Various observations have confirmed that the Galactic center, Sagittarius A* (Sgr A*), contains a super massive black hole of mass $\sim 4 \times 10^6 M_\odot$ (e.g., Ghez et al. 2008; Gillessen et al. 2009a,b). It has been found that Sgr A* emits radiation from radio through X-rays (see Melia & Falcke 2001; Melia 2007, for review) and even TeV γ -rays (Tsuchiya et al. 2004; Kosack et al. 2004; Aharonian et al. 2004; Albert et al. 2006). The bolometric luminosity of Sgr A* is $\sim 10^{36}$ erg s $^{-1}$ and the emission is dominated by radio. The spectral flux sharply falls off above $\nu \sim 10^{12}$ Hz (“the submillimeter bump”) (Zylka et al. 1995; Falcke et al. 1998). In the quiescent state, X-rays at low luminosities were also observed by *Chandra*, which obtained the X-ray luminosity of $L_X \approx 2.4 \times 10^{33}$ erg s $^{-1}$ in the 2 – 10 keV band (Baganoff et al. 2003). The quiescent state of Sgr A* can be described by a radiatively inefficient accretion flow (RIAF) model (Yuan et al. 2003) or a jet model (Falcke & Markoff 2000). These models ascribe the submillimeter bump to synchrotron radiation by thermal electrons in magnetic fields of ~ 30 G. The X-ray emission in the quiescent state is explained either by bremsstrahlung or by inverse Compton scattering in both RIAF (Yuan et al. 2003) and the jet models (Falcke & Markoff 2000).

Strong flares occur frequently in the X-ray band (Baganoff et al. 2001) and near-infrared (NIR) band (Genzel et al. 2003). The detailed properties of the flares of NIR and X-rays are reviewed in Dodds-Eden et al. (2009). X-ray and NIR flares occur simultaneously, with no significant delay (Eckart et al. 2004; Yusef-Zadeh et al. 2006). X-ray flares are always accompanied by NIR flares, although NIR flares may occur without an associated X-ray flare (e.g., Hornstein et al. 2007). It should be noted, however, that this might be instrumental, because the X-ray background in the Galactic center is proportionally larger than the NIR background and, thus, only bright X-ray flares are detected. The duration of NIR flare in the L' band (3.80 μm) observed in 2007 April 4 was about 100 minutes (Dodds-Eden et al. 2009). Simultaneously, *XMM-Newton* observed the flare in the X-ray band and the X-ray flare lasted about 60 minutes (Porquet et al. 2008). The L' -band light curve of the 2007 flare has sub-structural variations on a timescale of ~ 20 minutes. Dodds-Eden et al. (2009) attribute the NIR substructure to the fluctuation of the magnetic field.

Observations of polarization of the IR flares are broadly consistent with that the IR flares are synchrotron origin (e.g., Eckart et al. 2006a; Marrone et al. 2008; Dodds-Eden et al. 2009; Yusef-Zadeh et al. 2009). On the other hand, the emission mechanisms of the X-ray flares are still debated; upscattering of submillimeter photons (Markoff et al. 2001; Yusef-Zadeh et al. 2006), synchrotron self-Compton (SSC) scattering (Yuan et al. 2003; Eckart et al. 2004, 2006a,b; Sabha et al. 2010), synchrotron emission from high energy

electrons (Yuan et al. 2003, 2004; Dodds-Eden et al. 2009), or inverse Compton scattering of NIR photons by ~ 10 MeV electrons responsible for the quiescent radio-millimeter emission (Yusef-Zadeh et al. 2009). An orbiting hot spot model is also proposed (Broderick & Loeb 2005, 2006). This model requires the synchrotron cooling time longer than the orbital period to explain the light curve of NIR. However, the cooling time of X-ray emitting electrons is much shorter than the NIR emitting electrons. This makes the hot spot model inappropriate to the X-ray flare emission.

Dodds-Eden et al. (2009) explored the emission mechanisms of the 2007 IR/X-ray flare by various synchrotron and inverse Compton emission models. According to their model, SSC models need a large magnetic field such as 6000 G and a very small size of the flare emission region, e.g., $\sim 0.0013R_S$, where R_S is the Schwarzschild radius. The magnetic field is too large compared with the inferred value during the quiescent state, i.e., 10 - 30 G, and the size is too small to account for the flare timescale of 100 minutes. On the other hand, the flare is well explained by “powerlawcool” model, in which electrons with a power law with a cooling break emit IR and X-rays by synchrotron radiation. Recently, Sabha et al. (2010) explored SSC models that include parameter regions not considered by Dodds-Eden et al. (2009). Their model also requires a smaller source component size to give a sufficient inverse Compton scattering efficiency, so that multi-components are needed to obtain a broad time profile of a flare. Marrone et al. (2008) also constructed a SSC model of X-ray emission for a flare observed in 2006 July 17. The source size of their model is $\sim R_S$ and the strength of magnetic fields is 1.5 G. The source size and the magnetic fields are smaller than those of our model by a factor ~ 10 as shown in Section 3.

Because the origin of X-ray emission is still unclear as described above, in this paper we present a model that NIR and X-ray flares can be produced by synchrotron radiation from a single plasma blob. The simultaneity of NIR and X-ray flares favors a model of emission from a single region. The blob might be ejected from the region near the central black hole. As shown below, the size of the blob of our model is about $10 R_S$ and magnetic field is about 20 G. These values are consistent with the physical parameters of the accretion flow around the central black hole. In this model the flare duration is determined by the injection timescale of nonthermal electrons. The decay of the flares is owing to the radiative cooling and particle escape after turnoff of the injection of nonthermal electrons. In particular, we focus on the time-dependent behavior of the flare models. Because of various timescales such as cooling, injection, escape, etc., time-dependent simulations are necessary to investigate the flare properties in detail. It should be noted that most of the previous theoretical work on the flare emission has been restricted to the steady state models.

Although we do not consider adiabatic expansion in this paper, there are phenomena

suggesting the effects of adiabatic expansion. For example, Hornstein et al. (2007) found that their NIR measurements are consistent with a constant spectral index during a flare. Marrone et al. (2008) and Yusef-Zadeh et al. (2009), on the other hand, found that millimeter and submillimeter peaks delay the peak of NIR/X-ray flares. According to their models this delay is consistent with the adiabatic expansion of a self-absorbed source. The estimated expansion speed is much less than $0.1c$.

Our assumptions on the emission region are described in Section 2. Numerical results are given in Section 3. A summary of our results and discussion are given in Section 4. Throughout this paper, we assume 8 kpc as a Galactic center distance (Eisenhauer et al. 2003) and $4 \times 10^6 M_\odot$ as the central black hole mass (Ghez et al. 2008; Gillessen et al. 2009a,b).

2. Blob Model

We first assume that the emission region of the flares is a blob ejected from the central region around the black hole, e.g., from accretion flow (Wang, et al. 2000; Wang & Kusunose 2002; Yuan et al. 2009). For simplicity of numerical calculations, we assume that the blob is a uniform sphere with radius R and magnetic field B . While RIAF or a jet supplies the quiescent component of the spectral energy distribution (SED) of radiation, mainly in radio, the temporal ejection of a blob produces flare emission. Since the blob is launched from the inner edge or near the inner edge of the accretion flow, the blob speed might be at least mildly relativistic. However, we assume that the blob moves at nonrelativistic speed, so that the relativistic effects such as beaming are neglected. Because relativistic jets have not been observed from the region near Sgr A*, it is possible to neglect the effects of the motion of the blob as a first step of investigation.

In our simulations the injection of nonthermal electrons in the blob triggers flares. Shock acceleration in the blob or magnetic reconnection can supply such nonthermal electrons. We solve the kinetic equations of electrons and photons as in Kusunose et al. (2000) and Li & Kusunose (2000). We include the injection of nonthermal electrons, radiative cooling (synchrotron and inverse Compton scattering), and escape from the blob. The injection rate per unit volume and unit interval of γ , where γ is the electron Lorentz factor, is given by

$$q(\gamma) = \begin{cases} 0, & \text{if } \gamma < \gamma_{\min} , \\ K \gamma^{-p} \exp(-\gamma/\gamma_{\max}), & \text{if } \gamma \geq \gamma_{\min} , \end{cases} \quad (1)$$

where K , p , γ_{\min} , and γ_{\max} are parameters. The value of γ_{\max} can be a function of time, which allows different shapes of light curves. In our model described below, we assume that γ_{\max}

increases linearly with time to fit the flare light curves of 2007 April 4. The normalization factor, K , is determined by assigning the value of the injection rate per unit volume, i.e.,

$$q_{\text{inj}} = \int_{\gamma_{\text{min}}}^{\infty} q(\gamma) d\gamma. \quad (2)$$

A time-dependent q_{inj} model is also considered (see Section 3). The injection duration of nonthermal electrons, t_{inj} , and the escape timescale of electrons from the blob, t_{esc} , are also parameters. The emission mechanisms are synchrotron radiation by the nonthermal electrons and inverse Compton scattering of the synchrotron photons by the same electrons (SSC).

In this paper we do not consider Comptonization of external soft photons such as radiation from accretion flow. We discuss the validity of this assumption in Section 4. Furthermore, the adiabatic expansion of an initially optically thick blob is excluded, because there is no significant delay or asymmetry in the longer wavelength emission relative to the peak of the X-ray flare (Dodds-Eden et al. 2009).

3. Numerical Results

Numerical models are obtained for the parameters such as R , B , q_{inj} , p , γ_{min} , γ_{max} , t_{inj} , and t_{esc} . For a black hole mass $M_{\text{BH}} = 4 \times 10^6 M_{\odot}$, the Schwarzschild radius is $R_{\text{S}} = 2GM_{\text{BH}}/c^2 = 1.2 \times 10^{12}$ cm. The light crossing time of this size is $R_{\text{S}}/c \sim 40$ s. The particle escape occurs by advection, so that we set $t_{\text{esc}} \sim$ several R/c . In our model the injection duration is strongly related to the flare timescale. The values of parameters are determined by the SED of IR and X-ray flares and light curves. For this purpose, we use the data of the 2007 IR/X-ray flare given in Porquet et al. (2008) and Dodds-Eden et al. (2009).

3.1. Light Curves

In our model, the emission in both IR and X-ray bands is produced by synchrotron radiation. The maximum value of νF_{ν} of synchrotron emission appears at $\sim 10^{16}$ Hz, which is in between the IR and X-rays bands, where F_{ν} is the energy flux per unit frequency. The luminosity of X-rays is sensitive to the values of γ_{max} and t_{inj} . This is because X-rays are emitted by the electrons in the high energy end of the electron spectrum and the cooling time of those electrons is short. As soon as the injection rate of nonthermal electrons decreases, the X-ray luminosity declines. Because IR emitting electrons have longer cooling time than X-ray emitting electrons, the IR luminosity is more dependent on t_{esc} than the

X-ray luminosity. If t_{esc} is long enough, the X-ray emitting electrons begin to pile up as lower energy electrons that emit IR.

We first examine light curves of the IR and X-ray bands for various models. For models in this subsection, we assume that $R = 10^{13}$ cm, $B = 20$ G, $\gamma_{\text{min}} = 2$, $p = 1.3$, $t_{\text{inj}} = 8R/c$, and $t_{\text{esc}} = 5R/c$. The blob is initially empty at $t = 0$ and nonthermal electrons are injected for $t > 0$. In Figure 1, we present light curves in the L' ($3.8 \mu\text{m}$) and 2 – 10 keV bands for different models of γ_{max} and q_{inj} . When γ_{max} is fixed, high-energy electrons are injected instantly at $t = 0$. Then the light curves rise steeply (dotted lines). It is found for this model that the light curve of X-rays increases faster than that of IR, which is not in agreement with the flare of 2007 April 4. To obtain slower rise of the light curves, the time dependent γ_{max} is assumed as shown by the dashed lines. Here we assumed that γ_{max} increases linearly with time from 500 to 5×10^4 during $t = 0$ and t_{inj} . For $t > t_{\text{inj}}$ both models (the dotted and dashed lines) assume $q_{\text{inj}} = 0$. By fitting model light curves with the data of the flares, we found that the above models have shorter decline timescales than the observed one. We then assume that the injection rate decreases gradually after $t = t_{\text{inj}}$. As an example, we use a model with $q(\gamma) \propto \exp[-(t - t_{\text{inj}})/(\xi t_{\text{inj}})]$ for $t > t_{\text{inj}}$. In Figure 1, a model with $\xi = 0.25$ is shown by the solid lines (model A). In this model γ_{max} is constant for $t > t_{\text{inj}}$.

In Figures 2 and 3, we compare model light curves to the observed data for 2007 April 4. Here the model light curves are the same as shown by the solid lines in Figure 1, i.e., model A. The details of the model parameters are given in Table 1. The size of the blob R is 10^{13} cm and this corresponds to the light crossing time of 334 s. In this figure, the peak time of the luminosity of the model is shifted so that the model curves coincide with the observed light curves. We assumed the linear dependence of γ_{max} on time for $t < t_{\text{inj}}$ and the gradual decline of the injection rate for $t > t_{\text{inj}}$. The fact that IR and X-rays attain the peak flux almost simultaneously (Dodds-Eden et al. 2009) implies that the value of γ_{max} increases during the rising phase of the light curves, i.e., the acceleration of higher energy electrons is still underway in the early phase of the flare.

The cooling time of X-ray emitting electrons is ~ 11 s and much shorter than the escape time $t_{\text{esc}} \sim 1.7 \times 10^3$ s, if 10 keV of X-rays are assumed. On the other hand, NIR is emitted by electrons with $\gamma \sim 10^3$. The synchrotron cooling time of those NIR emitting electrons is comparable with t_{esc} , i.e., $t_{\text{cool}} \sim 2 \times 10^3$ s. Thus the cooling is effective in X-rays during the decay of the flare and the decline time of the X-ray light curve is shorter than that of NIR. The decline of the NIR light curve is regulated by both t_{cool} and t_{esc} . As shown in Figure 7, a bump appears at $\gamma \sim 10^3$ in the electron spectrum. This is because of balance between radiative cooling and escape.

3.2. Spectral Energy Distribution

We next show the evolution of the flare SED of model A and compare the model to the observations in Figure 4. The quiescent model by Yuan et al. (2003) is also shown for comparison. The maximum flare luminosity is 5.0×10^{37} erg s⁻¹ at $t = 9R/c$. This luminosity is much higher than the submillimeter luminosity in the quiescent state, but this flare does not strongly affect the spectrum in the submillimeter wavelength. During the rising phase, synchrotron emission becomes luminous and attains the peak at $t \sim 8R/c$. The peak frequency increases because γ_{\max} increases for $t < t_{\text{inj}}$. While the emission decays, the spectrum in the IR and X-ray bands become flatter and a dip appears at $\sim 10^{15}$ Hz.

It is noted that the SSC component appears in the GeV region, whose intensity might be too small to be observed. However, other sets of parameter values allow a stronger GeV flux as shown below.

Since the number of parameters is large and observed data are few, there is uncertainty in determining the parameter values to fit the data. We show another model (model B) with $p = 1.8$ in Figure 5. When p has a larger value, the value of γ_{\min} should be larger for the radio flare not to exceed the quiescent radio emission. When the value of p is larger and the value of γ_{\min} is fixed, there are more electrons with lower energy for the same IR and X-ray luminosities as the observed data. This constraint on γ_{\min} may be not strong, if flares in radio occur simultaneously.

As shown in Figure 4, our model predicts the emission in the GeV band, which is produced by inverse Compton scattering of IR-optical photons, i.e., SSC process. The luminosity in the GeV band is not strongly constrained in our model. In Figure 6, we show a model with a larger luminosity in the GeV band (model C). A smaller value of the magnetic field and a higher injection rate produce a luminous SSC component. The difference of SEDs in Figures 4 and 6 also appears in the IR band of the decaying phase. In Figure 4 the IR spectrum becomes flat after $t \sim 12R/c$, while that in Figure 6 keeps hard spectral shape.

3.3. Electron Spectrum and Energetics

The time evolution of the electron spectrum of model A is shown in Figure 7. The number density of electrons increases for $t < t_{\text{inj}}$ because of injection. For $t > t_{\text{inj}}$, the injection rate decreases exponentially with time. The higher energy electrons decrease because of radiative cooling. Also on timescale t_{esc} , electrons escape from the blob.

The time evolution of the energy densities of the radiation u_{rad} and the kinetic energy

of electrons u_e is shown in Figure 8 for model A. In our model the magnetic field is assumed to be constant. The energy content is dominated by the magnetic energy density u_B , i.e., $u_B/u_e \sim 16$ at $t \sim 8R/c$. This is in contrast with blazar models, where the kinetic energy of nonthermal electrons/positrons dominates over the magnetic energy (Kino et al. 2002). Blazars are relativistic jets aligned with the line of sight and the relativistic beaming effect enhances the luminosity, while our model of Sgr A* does not have relativistic motion. It should be also noted that blazars have a luminous SSC or external Compton component in the γ -ray band, while model A has only a weak SSC component. When the SSC component is more luminous as in model C, the electron energy dominates over the magnetic energy, i.e., $u_B/u_e \sim 0.1$ at $t \sim 8R/c$.

4. Summary and Discussion

We calculated the SEDs and light curves from a blob as a model of the IR and X-ray flares observed from Sgr A*. Because we performed time-dependent calculations, it was possible to study the evolution of radiation and electron spectra in detail, which is different from most of previous work. Our model assumes that IR and X-rays are emitted by synchrotron radiation of nonthermal electrons injected in the blob. This model explains the characteristics of 2007 April 4 flare in IR/X-rays such as (1) the simultaneity of the X-ray and IR flares, (2) the steeper decline of the X-ray flare than the IR flare, (3) the flare timescale of 100 minutes. The flare timescale in our model is mainly determined by the injection time of nonthermal electrons, which is related to particle acceleration mechanisms and to be studied in future work. To compare the light curves we assumed that the value of γ_{\max} increases linearly with time. If the value of γ_{\max} is fixed during injection, our model does not explain the simultaneity of the X-ray and IR flares. The higher energy electrons responsible for X-ray emission are thus being accelerated in the rising phase of the flare.

We compared the SEDs of different models. While model A has a faint SSC component in γ -rays and a larger value of u_B/u_e , model C has a bright SSC one and a smaller value of u_B/u_e . If model C is applicable, we will observe γ -rays in the GeV band. Future observations in the GeV band will constrain the model parameters as well as the energetics in the flare regions. Because the blob might be ejected from RIAF by magnetohydrodynamic processes and nonthermal electrons are accelerated in the collisionless shock, the observations of GeV γ -rays will clarify the origin of the blobs and the particle acceleration mechanisms.

The spectral index of NIR is almost constant during a flare in model C, while the spectrum becomes flatter during the decay in models A and B. In model C, the cooling time is longer than that of models A and B, because the magnetic field is weaker. Then only

escape time, which is independent of electron energy, regulates the decay of the NIR flare.

Previous work mainly modeled the SED of flares by steady state models and did not utilize the data of light curves. Time-dependent models were recently published by Sabha et al. (2010). They assumed SSC for X-ray flares and combined adiabatic expansion to account for light curves of 2007 April 4. To fit the data six source components are needed. While it is possible to attribute the IR substructure to those multi-components of sources, it seems difficult to produce many emission regions coherently to cause flares.

It is known that IR flares sometimes occur without X-ray flares. This might be owing to a small value of γ_{\max} because of inefficient acceleration, rapid radiative cooling, or adiabatic cooling. If, for example, a blob is close to RIAF and external Compton scattering is important, synchrotron X-ray flares are suppressed. If this is the case, the effect of external Compton scattering appears as weak X-ray flares or hard spectral X-ray emission. This is because when synchrotron X-ray flares are absent, the kinetic energy of electrons with $\gamma \gtrsim 10^3$ are given to the RIAF photons with $\nu \sim 10^{12}$ Hz, yielding X-rays with $\nu \gtrsim 10^{18}$ Hz. The intensity of these X-rays depends on the distance of the blob from RIAF.

We neglected the effect of the radiation from the RIAF in the flare emission spectra. By inverse Compton scattering of submillimeter photons with 10^{12} Hz, electrons with $\gamma_{\max} \sim 10^4$ produces gamma-rays with ~ 1 MeV. If the submillimeter emission ($L \sim 3.85 \times 10^{35}$ erg s^{-1}) is received by the blob, the energy density of the submillimeter photons in the blob is $\sim 1.8 \times 10^{-2}$ erg cm^{-3} . Here we assumed that the photon density decreases as the square of the distance, that the distance of the blob from the submillimeter emission region is 1 AU, and that the submillimeter emission is isotropic. This energy density should be compared with that of synchrotron photons in the blob, ~ 0.3 erg cm^{-3} at $t \sim 8R/c$ (model A). Thus external Compton scattering of submillimeter photons is negligible, if the distance is greater than about 1 AU.

After completion of this work, we noticed a paper by Dodds-Eden et al. (2010). They solved a kinetic equation of electrons and obtained time-dependent flare spectra of synchrotron radiation: Note that they did not calculate SSC spectra. In their work flares are caused by the change in the injection rate and magnetic fields, while we assumed the change in the injection rate and γ_{\max} .

REFERENCES

- Aharonian, F. et al. 2004, A&A, 425, L13
 Albert, J. et al. 2006, ApJ, 638, L101

- Baganoff, F. K., et al. 2001, *Nature*, 413, 45
- Baganoff, F. K., et al. 2003, *ApJ*, 591, 891
- Broderick, A. E., & Loeb, A. 2005, *MNRAS*, 363, 353
- Broderick, A. E., & Loeb, A. 2006, *MNRAS*, 367, 905
- Dodds-Eden, K., et al. 2009, *ApJ*, 698, 676
- Dodds-Eden, K., et al. 2010, *ApJ*, 725, 450
- Eckart, A. et al. 2004, *A&A*, 427, 1
- Eckart, A. et al. 2006a, *A&A*, 450, 535
- Eckart, A. et al. 2006b, *A&A*, 455, 1
- Eisenhauer, F., et al. 2003, *ApJ*, 597, L121
- Falcke, H., & Markoff, S. 2000, *A&A*, 362, 113
- Falcke, H., et al. 1998, *ApJ*, 499, 731
- Genzel, R., et al. 2003, *Nature*, 425, 934
- Ghez, R., et al. 2008, *ApJ*, 689, 1044
- Gillessen, S., et al. 2009a, *ApJ*, 692, 1075
- Gillessen, S., et al. 2009b, *ApJ*, 707, L114
- Hornstein, S. D., et al. 2007, *ApJ*, 667, 900
- Kino, M., Takahara, F., & Kusunose, M. 2002, *ApJ*, 564, 97
- Kosack, K. et al. 2004, *ApJ*, 608, L97
- Kusunose, M., Takahara, F., & Li, H. 2000, *ApJ*, 536, 299
- Li, H., & Kusunose, M. 2000, *ApJ*, 536, 729
- Markoff, S., Falcke, H., Yuan, F., & Biermann, P. L. 2001, *A&A*, 379, L13
- Marrone, D. P., et al. 2008, *ApJ*, 682, 373

- Melia, F. 2007, *The Galactic Supermassive Black Hole* (Princeton, NJ: Princeton Univ. Press)
- Melia, F., & Falcke, H. 2001, *ARA&A*, 39, 309
- Porquet, D. et al. 2008, *A&A*, 488, 549
- Sabha, N. et al. 2010, *A&A*, 512, A2
- Tsuchiya, K. et al. 2004, *ApJ*, 606, L115
- Wang, J.-M., Yuan, Y.-F., Wu, M., & Kusunose, M 2000, *ApJ*, 541, L41
- Wang, J.-M., & Kusunose, M. 2002, *ApJS*, 138, 249
- Yuan, F., Lin, J., Wu, K., & Ho, L. C. 2009, *MNRAS*, 395, 2183
- Yuan, F., Quataert, E., & Narayan, R. 2003, *ApJ*, 598, 301
- Yuan, F., Quataert, E., & Narayan, R. 2004, *ApJ*, 606, 894
- Yusef-Zadeh, F., et al. 2006, *ApJ*, 644, 198
- Yusef-Zadeh, F., et al. 2009, *ApJ*, 706, 348
- Zhao, J.-H., et al. 2003, *ApJ*, 586, L29
- Zylka, R., et al. 1995, *A&A*, 297, 83

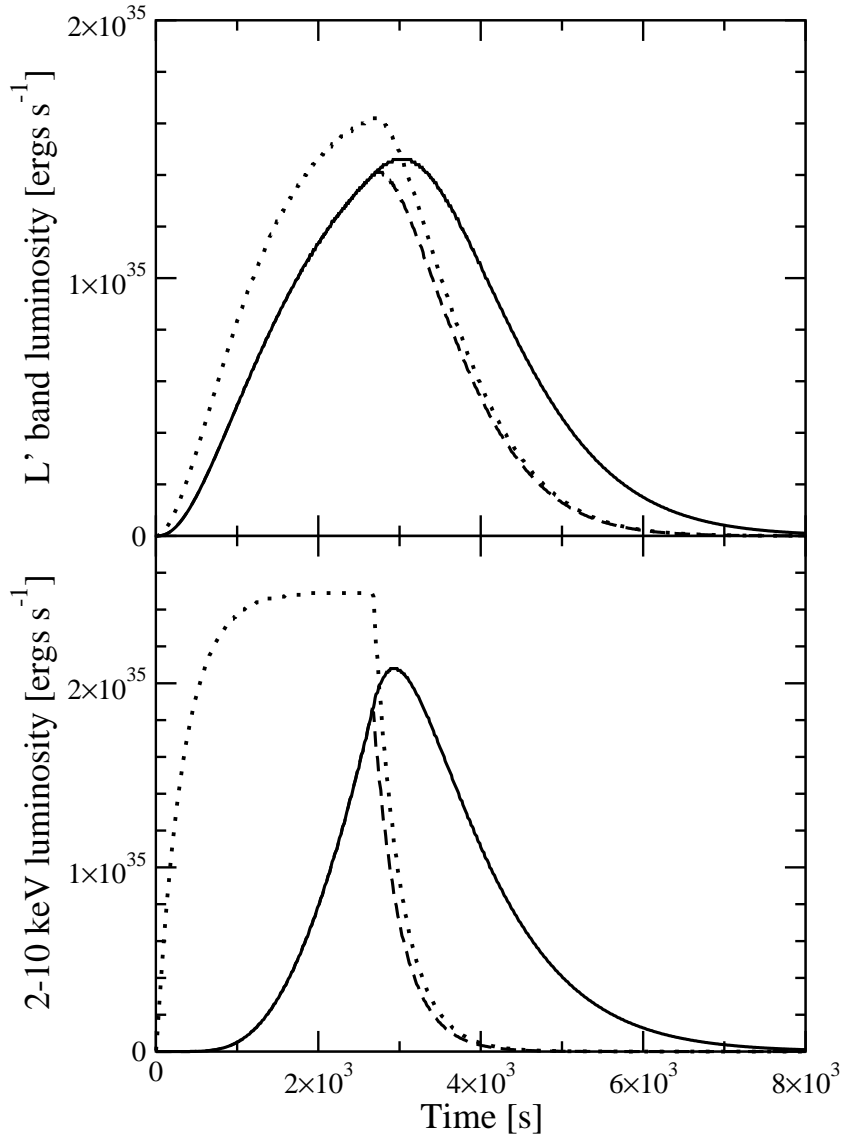


Fig. 1.— Light curves of the L' band ($3.8\mu\text{m}$) and the 2 – 10 keV band for various models. A model with a fixed value of $\gamma_{\text{max}} = 5 \times 10^4$ is shown by dotted lines. The dashed lines are for a model with a time dependent γ_{max} . Here we assume that γ_{max} increases linearly from 500 to 5×10^4 during $t = 0$ and t_{inj} , where $t_{\text{inj}} = 2.7 \times 10^3$ s. Both models assume that the injection is at a constant rate and stops at $t = t_{\text{inj}}$. A model with a time dependent injection is shown by solid lines. This model assumes that q_{inj} is constant for $t < t_{\text{inj}}$ and decreases as $q_{\text{inj}} \propto \exp[-(t - t_{\text{inj}})/(0.25t_{\text{inj}})]$ for $t > t_{\text{inj}}$. The value of γ_{max} increases linearly as for the model shown by the dashed lines. For all these models, $R = 10^{13}$ cm, $B = 20$ G, $\gamma_{\text{min}} = 2$, $p = 1.3$, $t_{\text{inj}} = 8R/c$, and $t_{\text{esc}} = 5R/c$ are used.

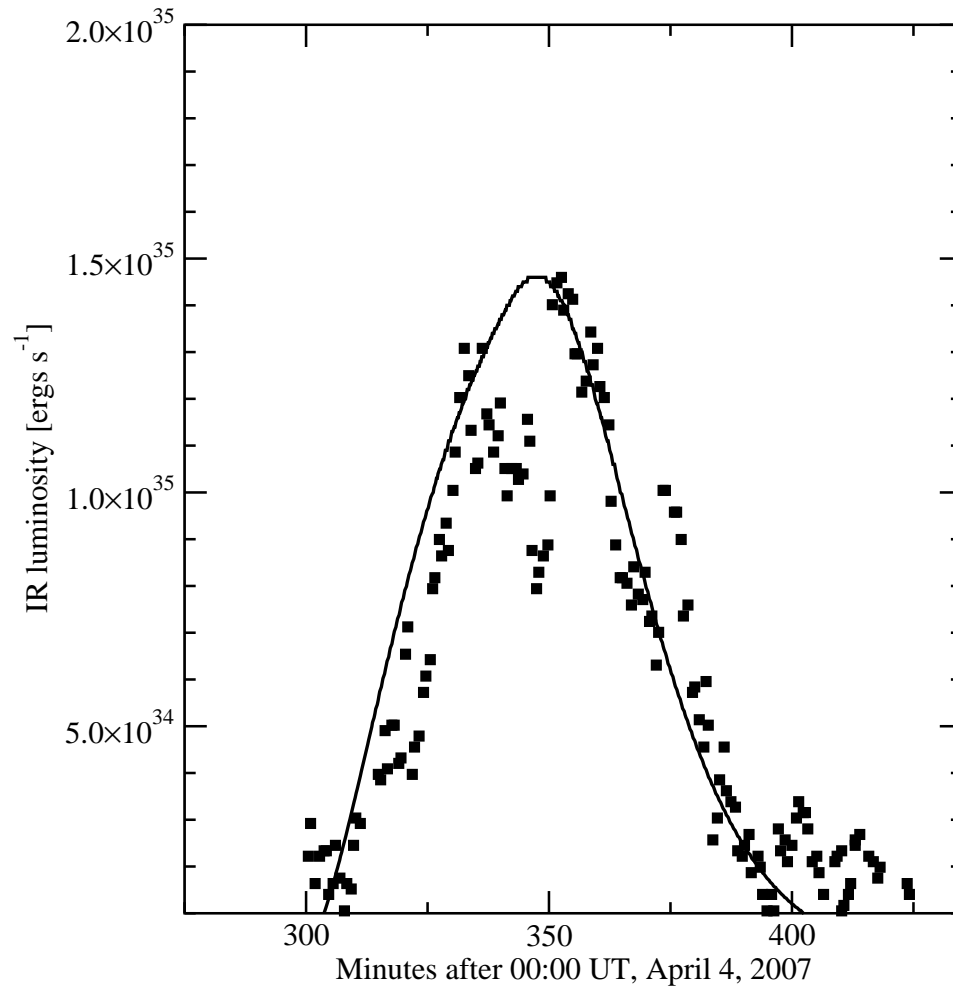


Fig. 2.— Light curves of the L' band. The flare data of the L' band (filled squares) are from Dodds-Eden et al. (2009). The solid line depicts model A. The value of γ_{\max} increases linearly with time from 500 up to 5×10^4 . In Figures 2 and 3, the peak time of model light curves are shifted so that the peak time coincides with the observed peak time.

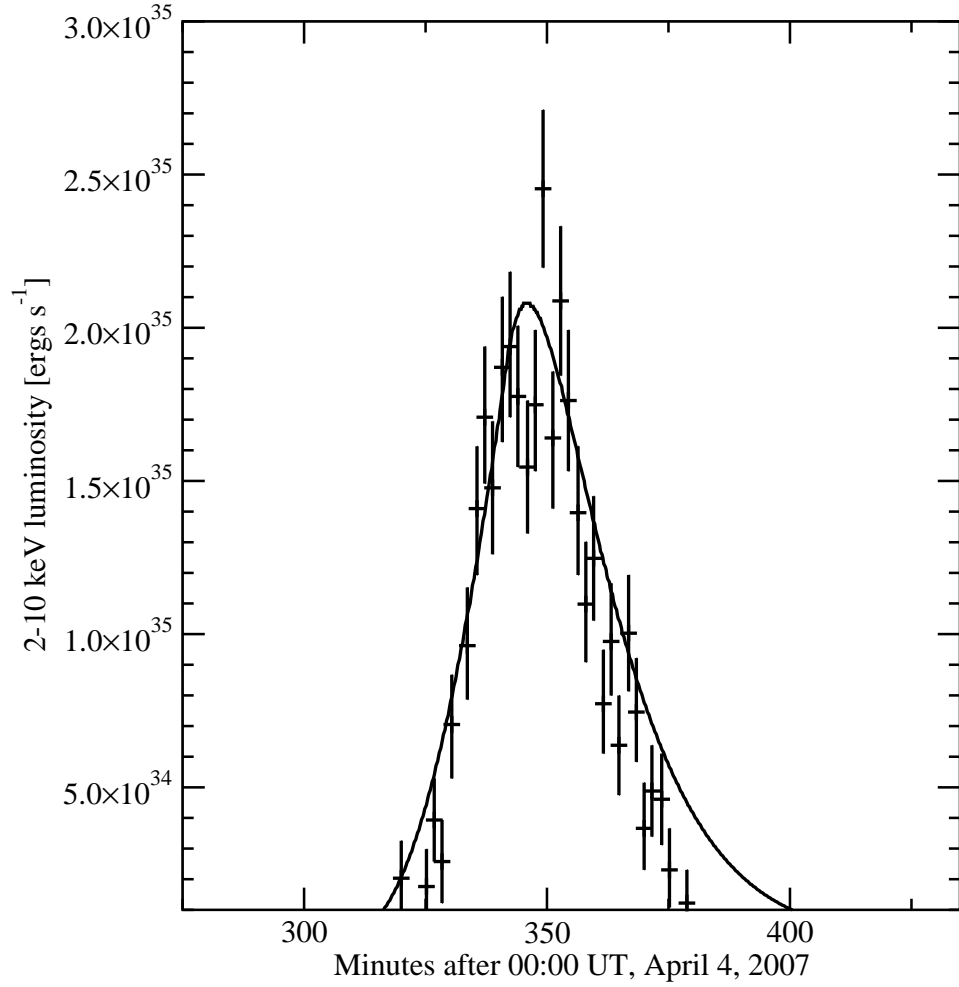


Fig. 3.— Light curves of the 2 – 10 keV band. The flare data of the X-ray band (pluses) are from Porquet et al. (2008). Model A is shown by a solid line.

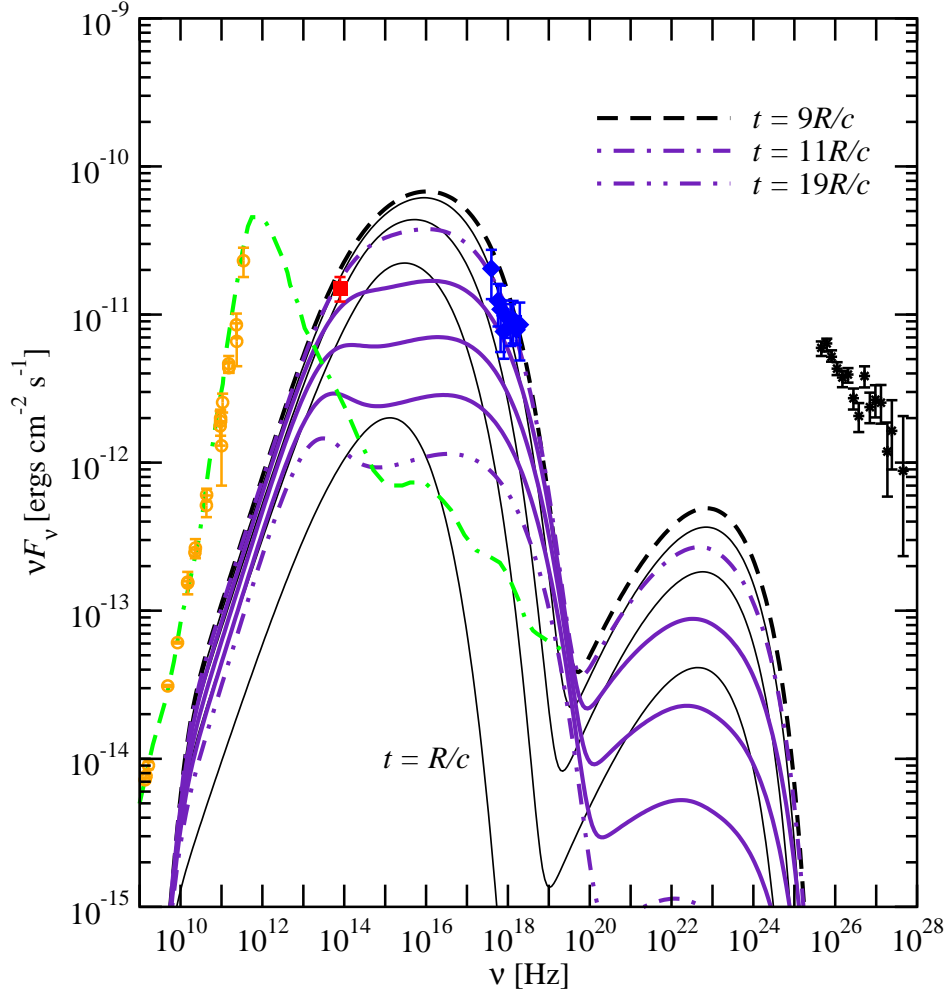


Fig. 4.— Time evolution of the SED of model A. The SEDs are shown for $t = R/c - 19R/c$ at every $2R/c$. SEDs in the rising phase are shown by thin lines and those in the decaying phase by thick lines. Radio to submillimeter measurements are for the quiescent state (Markoff et al. 2001; Zhao et al. 2003) (open circles). The flaring state in NIR (filled square) is taken from Dodds-Eden et al. (2009). The X-ray flare data (filled diamonds) are from Porquet et al. (2008). TeV emission (Aharonian et al. 2004) is also shown by asterisks. The quiescent state RIAF model by Yuan et al. (2003) is shown by a dash-dash-dotted line for comparison.

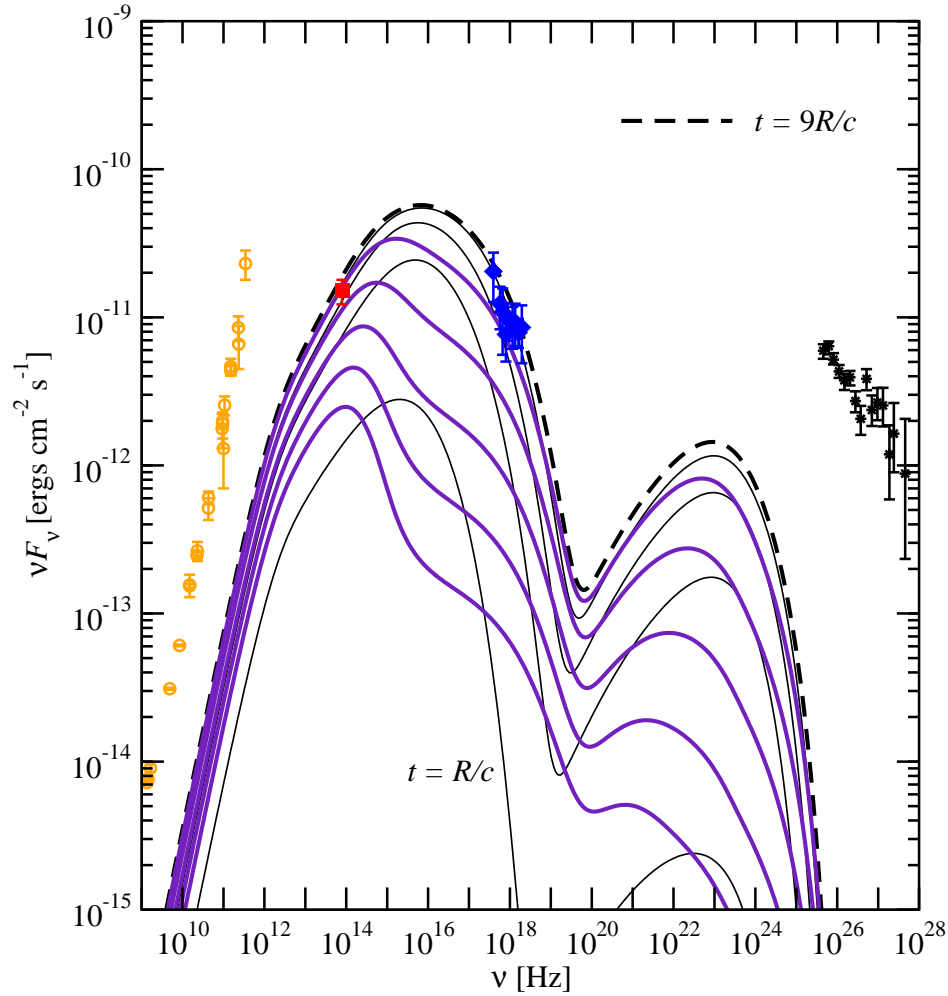


Fig. 5.— Time evolution of the SED of model B with $p = 1.8$. Here, $\gamma_{\min} = 2 \times 10^2$ is assumed. The value of γ_{\max} is increased from 1.3×10^3 up to 1.3×10^5 linearly with time during $t = 0$ and t_{inj} . SEDs in the rising phase are shown by thin lines and those in the decaying phase by thick lines.

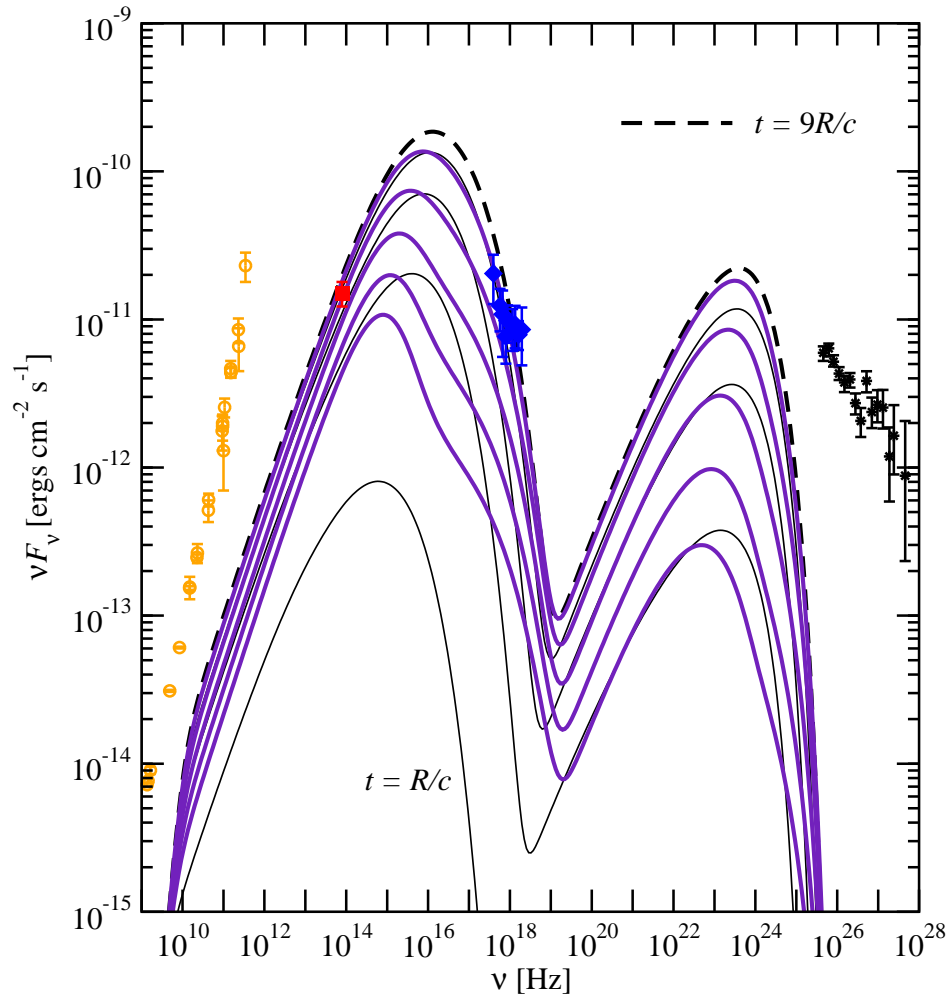


Fig. 6.— Time evolution of the SED with a luminous SSC component (model C). Here, $B = 5$ G and $q_{\text{inj}} = 7.5$ are assumed. SEDs in the rising phase are shown by thin lines and those in the decaying phase by thick lines.

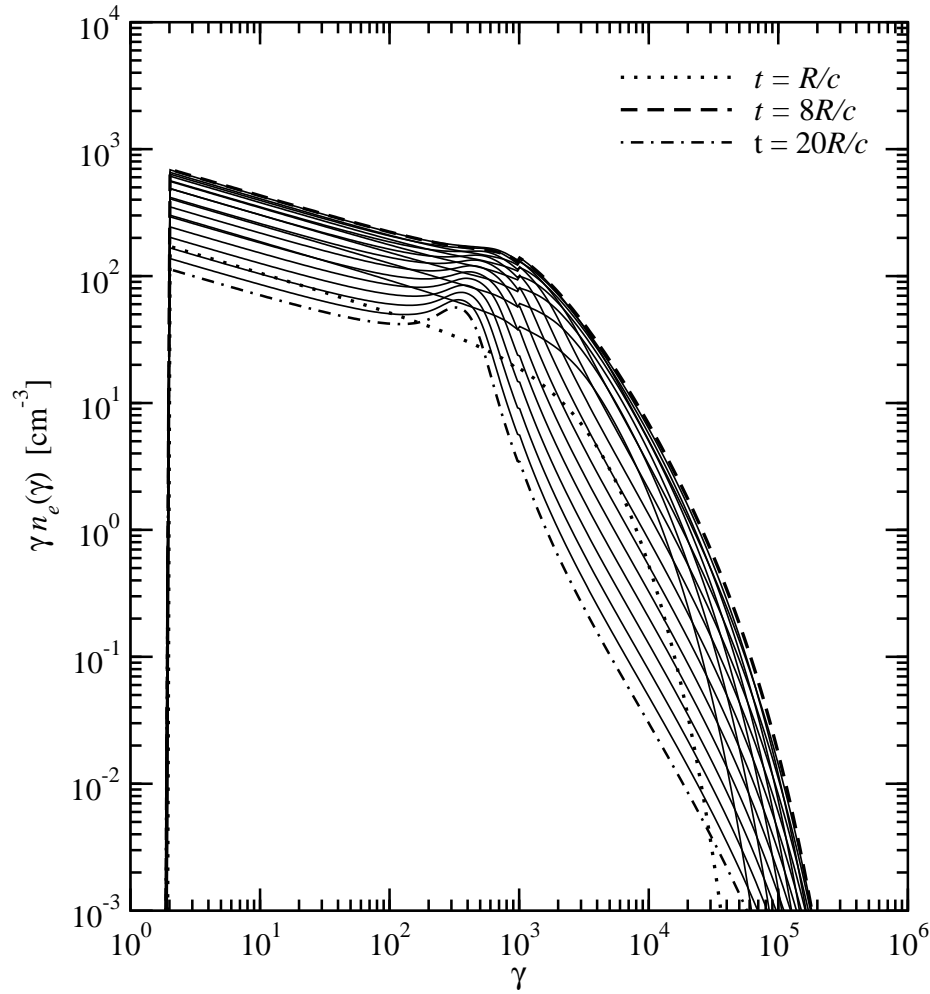


Fig. 7.— Time evolution of the electron spectrum of model A. Here, $n_e(\gamma)$ is the electron number density per unit γ . The spectra are shown for every R/c . After $t = 8R/c$, the injection rate decreases exponentially.

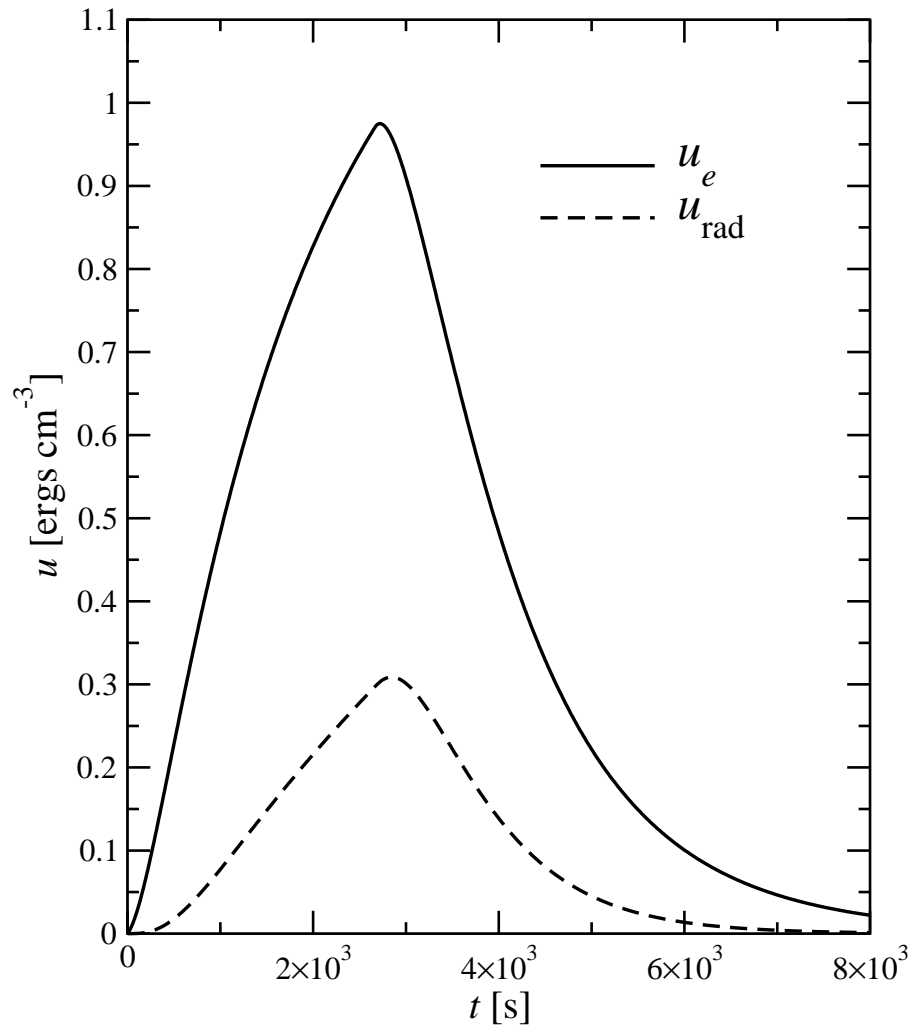


Fig. 8.— Time evolution of the energy densities of electrons (solid) and radiation (dashed). This model assumes that the magnetic energy density is constant, i.e., $B^2/(8\pi) = 15.9 \text{ erg cm}^{-3}$ with $B = 20 \text{ G}$.

Table 1. Parameters

Model	$B(\text{G})$	p	γ_{\min}	γ_{\max}	$q_{\text{inj}}(\text{cm}^{-3} \text{ s}^{-1})$
A	20	1.3	2	5×10^4	1.6
B	10	1.8	2×10^2	1.3×10^5	1.1
C	5	1.3	2	5×10^4	7.5

Note. — All models assume $R = 10^{13}$ cm, $t_{\text{inj}} = 8R/c$, and $t_{\text{esc}} = 5R/c$. The increase of γ_{\max} during electron injection time is assumed and the values of γ_{\max} listed above are those at $t = t_{\text{inj}}$.